*Journal of Ceramic Processing Research. Vol. 21, No. 2, pp. 208~212 (2020)*
*(Received 1 November 2019, Received in revised form 10 January 2020, Accepted 17 January 2020)*
*https://doi.org/10.36410/jcpr.2020.21.2.208*

J O U R N A L O F
**Ceramic Processing Research**

# Effect of $La_{0.8}Ca_{0.2}Cr_{0.9}Co_{0.1}O_{3-\delta}$ infiltration on the LCCC-YSZ layer as an interconnector material in solid oxide fuel cells

**Ho-Chang Lee, Jiwon Lee, Jung-A Lee, Young-Woo Heo, Joon-Hyung Lee* and Jeong-Joo Kim***
*School of Materials Science and Engineering, Kyungpook National University, Daegu 41566, Republic of Korea*

**Full densification of the interconnector $La_{0.8}Ca_{0.2}Cr_{0.9}Co_{0.1}O_{3-\delta}$ (LCCC) layer is hardly achieved when it is screen-printed and cofired on a pre-sintered NiO-YSZ (yttria-stabilized zirconia, 8YSZ) substrate. In this study, the LCCC precursors with different concentrations and viscosities were prepared and infiltrated into the LCCC-YSZ layer. The phase development process and densification behavior of the LCCC were analyzed, and the optimum conditions for full densification are suggested. Through the research, we propose a method for manufacturing a dense LCCC interconnector layer.**

**Keywords: Sintering, Ceramics, Interconnector, Sol-gel preparation, Infiltration.**

## Introduction

Solid oxide fuel cells (SOFCs) consist of electrolytes, anodes, and interconnectors. The interconnector acts as a physical barrier to avoid any contact between the reducing and oxidizing atmospheres. The interconnector must exhibit excellent electrical conductivity and adequate dimensional, microstructural, chemical, and phase stability at operating temperatures of approximately 800 °C under both reducing and oxidizing atmospheres. Furthermore, the thermal expansion coefficient of the interconnector should match with those of the electrodes and electrolyte [1-3].

Only a few oxide systems can satisfy the rigorous requirements of SOFC interconnectors. $LaCrO_3$ is currently the most widely used material [4, 5] for doping at either La or Cr sites, or at both sites [5], and various synthesis methods have been used to increase the sinterability [6-8]. Owing to their similar ionic radii, Sr and Ca tend to replace La ions, whereas Mg, Fe, Ni, Cu, and Co tend to replace Cr ions.

It has been previously reported that the doping of $LaCrO_3$ with Ca and Co ($La_{0.8}Ca_{0.2}Cr_{0.9}Co_{0.1}O_{3-\delta}$, LCCC) greatly improves its density. However, significant tensile stress was observed on the LCCC layer when an LCCC interconnector was screen-printed and cofired on a pre-sintered NiO-YSZ (yttria-stabilized zirconia, 8YSZ) substrate, which resulted in the densification retardation of the LCCC layer. This phenomenon could be overcome by the addition of YSZ, which is a constituent of the anode, to the LCCC [9].

In this study, the ethylene glycol-based LCCC solution was infiltrated into the LCCC-YSZ (LCCC70 wt.% − YSZ30 wt.%) interconnector layer to enhance its density. The LCCC concentration of the precursor solution and the heating rate during sintering were controlled. It was found that the viscosity of the solution varied with synthesis time because a cross-linking reaction occurred simultaneously during polymerization. When the synthesis was conducted at a high temperature, the sol became volatile. Upon prolonging the synthesis period, the LCCC concentration of the precursor solution changed and affected the viscosity. Following the infiltration, the local temperature difference during sintering caused a change in the viscosity and affected the final microstructure.

## Experimental

The precursor solutions used for the infiltration process were prepared from $La(NO_3)_3 \cdot 6H_2O$ (Alfa Aesar, 99.9%), $Ca(NO_3)_2 \cdot 4H_2O$ (Alfa Aesar, 99.9%), $Cr(NO_3)_3 \cdot 6H_2O$ (Alfa Aesar, 99.9%), and $Co(NO_3)_3 \cdot 6H_2O$ (Junsei, 99.9%). The concentration of the precursor solution was 0.2 M [10-11] and the atomic ratio of La:Ca:Cr:Co was 0.8:0.2:0.9:0.1. The starting materials were dissolved in distilled water, followed by the addition of ethylene glycol and nitric acid. The precursor solution used for the infiltration was heated at 95 °C and stirred for durations varying from 1 to 5 d. Each precursor solution was heat-treated at 1,400 °C. The LCCC concentration was determined by measuring the mass of the remaining powder. An X-ray diffractometer (X'Pert PRO, PANalytical) with Cu K*a* radiation was used to monitor the phase transformation of the precursor solutions that were heat-treated from 200 to 1,400 °C.

*Corresponding author: Jeong-Joo Kim
Tel.: +82–53–950–5635; Fax: +82–53–950–5645
E-mail: jjkim@knu.ac.kr
*Co-corresponding author: Joon-Hyung Lee
Tel.: +82–53–950–7512; Fax: +82–53–950–5645
E-mail: joonlee@knu.ac.kr

The substrate was prepared using NiO (Sumitomo Chemical Co., 99.9%) and YSZ (Unitec, 99.9%) powders as raw materials. The homogeneously mixed powder with a weight ratio of NiO:YSZ = 56:44 formed substrates with thickness of 1 mm, which were then pre-sintered at 1,250 °C. The LCCC-YSZ paste was printed onto a NiO–YSZ substrate using a 150-mesh screen. The bilayer specimens were cofired at 1,400 °C for 2 h in air. To investigate the effect of infiltration in the interconnector layer, each precursor solution was impregnated on the sintered bilayer specimens, which were then sintered at 1,400 °C for 2 h in air at a heating rate of either 1 or 5 °C/min. The cross-section and surface of each sample were examined using a field-emission scanning electron microscope (FE-SEM, JSM-6701F, JEOL) with 10 kV and 10 μA. The viscosities of each solution were measured at room temperature using a rotational rheometer (MCR301, Anton Paar) with 50 mm diameter of the plate and 1 mm of the gap between the plates.

## Results and Discussion

Fig. 1 shows the microstructures of the cross-section and top surface of the screen-printed LCCC-YSZ layer on the NiO-YSZ anode substrate. There was no reaction between NiO-YSZ and the LCCC-YSZ paste at 1,400 °C, as shown in the XRD patterns in a previous study [9]. The calculated porosity was ~36% based on cross-sectional analysis (Fig. 1(a)) and the pores were seemingly continuously connected. The LCCC mixture with 30 wt.% YSZ was well attached to the NiO-YSZ substrate; however, the porosity of the material was still too high to be used as an interconnector in an SOFC.

Table 1 shows the LCCC concentrations calculated based on the weight loss after heat treatment at 1400 °C, and room temperature viscosity after different mixing periods. When the synthesis time was extended from 1 d to 5 d, there was a 20-fold increase in the viscosity from 20.1 to 463.2 mPa·s and the LCCC concentration doubled from 9% to 19%. The increase in LCCC concentration was attributed to the oxidation of ethylene glycol. Ethylene glycol was transformed into oxalic acid and an esterification reaction occurred between the oxalic acid and the remaining ethylene glycol; this reaction led to volume reduction because of the dehydration of the solvent [10-11]. The increased viscosity of the precursor solution resulted in a continuous increase in the LCCC concentration, and the polymer chain length also increased in accordance with the polymerization. Plonczak et al. have previously reported that the viscosity changes in ethylene glycol-based $Ce_{0.9}Gd_{0.1}O_{1.95}$ as a function of time were a result of concentration changes occurring together with the proceeding polymerization reaction [12].

Fig. 2 shows the X-ray diffraction patterns of the LCCC precursor heat-treated from 200 to 1,400 °C. No crystallization occurred in the LCCC precursor that was heat-treated at 200 °C. The LCCC precursors heat-treated at 400 and 600 °C contained $LaCrO_4$ as the main phase and $La_2CrO_6$ as a secondary phase. When the LCCC precursor was heat-treated at 800 °C, $CaCrO_4$ was observed as a secondary phase in addition to $LaCrO_3$ as the main phase. It was reported that $LaCrO_4$ transforms into $LaCrO_3$ at 700 °C [13] and the $CaCrO_4$ secondary phase also forms in the temperature range of 800-1,000 °C in Ca-doped $LaCrO_3$ [13-15]. In the case of the LCCC precursor heat-treated at 1,400 °C, a single phase of $LaCrO_3$ was formed; the $CaCrO_4$ phase had likely dissolved into the LCCC lattice during heat treatment.

Fig. 3 presents the cross-section and top surface images of the samples sintered at 1,400 °C for 2 h at

**Table 1.** LCCC concentration in the LCCC precursor annealed at 1,400 °C and room temperature viscosity as a function of the stirring time at 95 °C.

| Sol stirring time (day) | Viscosity (mPa·s) | Solute concentration (%) |
|---|---|---|
| 1 | 20 | 8.8 |
| 3 | 61.2 | 12.26 |
| 5 | 463.2 | 19.01 |

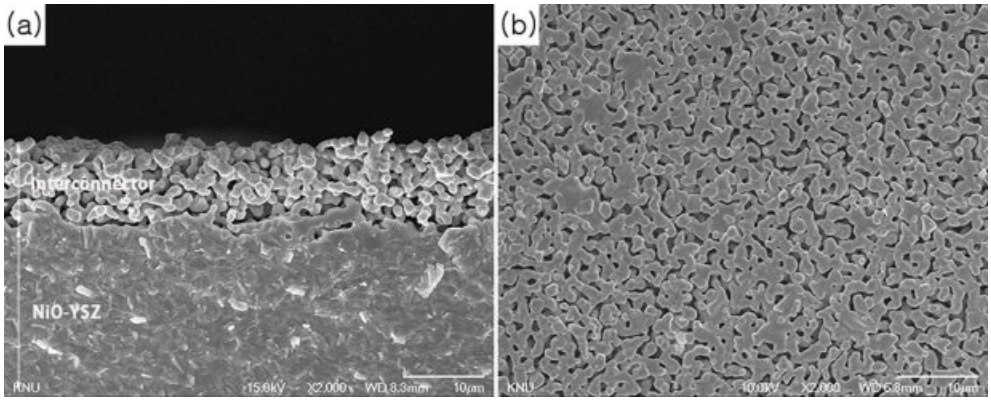


**Fig. 1.** Microstructures of the bilayers co-fired at 1,400 °C for 2 h: (a) cross-section and (b) top surface.

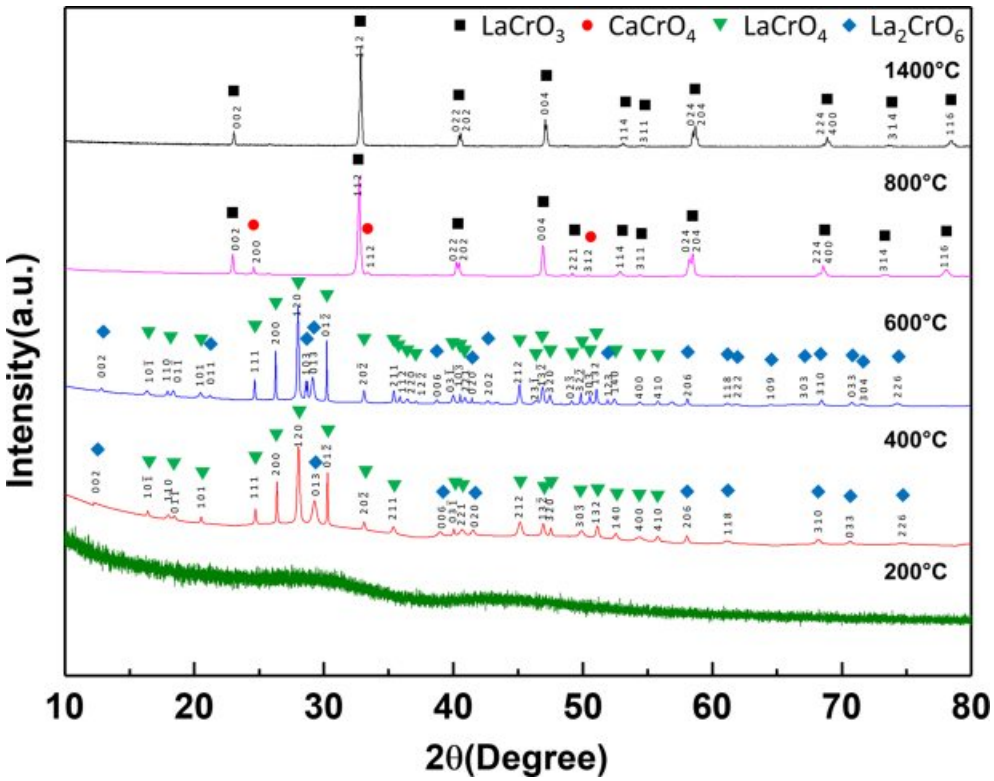


**Fig. 2.** X-ray diffraction patterns of the precursor heat-treated at various temperatures.

heating rates of 1 °C/min and 5 °C/min. Prior to sintering, each precursor solution was screen-printed on the porous LCCC-YSZ layer as shown in Fig. 1. Fig. 3(a) shows the microstructure of the specimen that was infiltrated by the 9% LCCC precursor solution. It was found that the interconnector layer was densified to half its depth. Fig. 3(c) shows the fully densified microstructure of the specimen that was infiltrated by the 12% LCCC precursor solution and the top surface shown in Fig. 3(d) is also very dense. Fig. 3(e) shows the microstructure of the specimen infiltrated by the 19% LCCC precursor solution. The interconnector layer had a porous structure in this case because the precursor solution did not infiltrate into the LCCC-YSZ layer as a result of its high viscosity.

Fig. 3(g) shows the microstructure of the specimen infiltrated by the 12% LCCC precursor solution and heated at 1,400 °C with a heating rate of 5 °C/min to slow down the gelation of the precursor solution. The top layer was dense, but the bottom layer was porous. It was rationalized that the differences in the viscosity and polymer molecular chain length between the top and bottom layers of the interconnector could be attributed to the rapid heating rate. The precursor on the top layer dried faster when the heating rate is faster than slower. In addition, gelation occurred continuously and larger clusters were formed via polymerization, a result of the esterification reaction and evaporation of water during the reaction that led to a higher solute concentration. Once the precursor solution infiltrated the layers, the residual precursor solution could no longer penetrate because of high viscosity and long polymer chain lengths.

The fully densified microstructure in Fig. 3(c) was a result of the slow heating rate, which ensured the low viscosity and short molecular chain length of the polymer. It was rationalized that the solution present at the bottom of the sample would also move slightly upwards because of the capillary force generated when the remaining precursor solution transformed into the xerogel.

## Conclusions

Porous LCCC-YSZ (LCCC 70 wt.%−YSZ 30 wt.%) was formed on a NiO-YSZ anode substrate and subsequently treated with an ethylene glycol-based LCCC solution to enhance its density. At the heating rate of 1 °C/min, the precursor solution with an LCCC concentration of 12% permeated the entire interconnector layer. When the heating rate was 5 °C/min, a dense region was formed at the top layer. It is considered that the precursor solution remaining on the surface after screen-printing had a higher viscosity and longer molecular length than that on the bottom layer. The solution dried rapidly at the surface during the rapid heating rate and further infiltration did not occur.

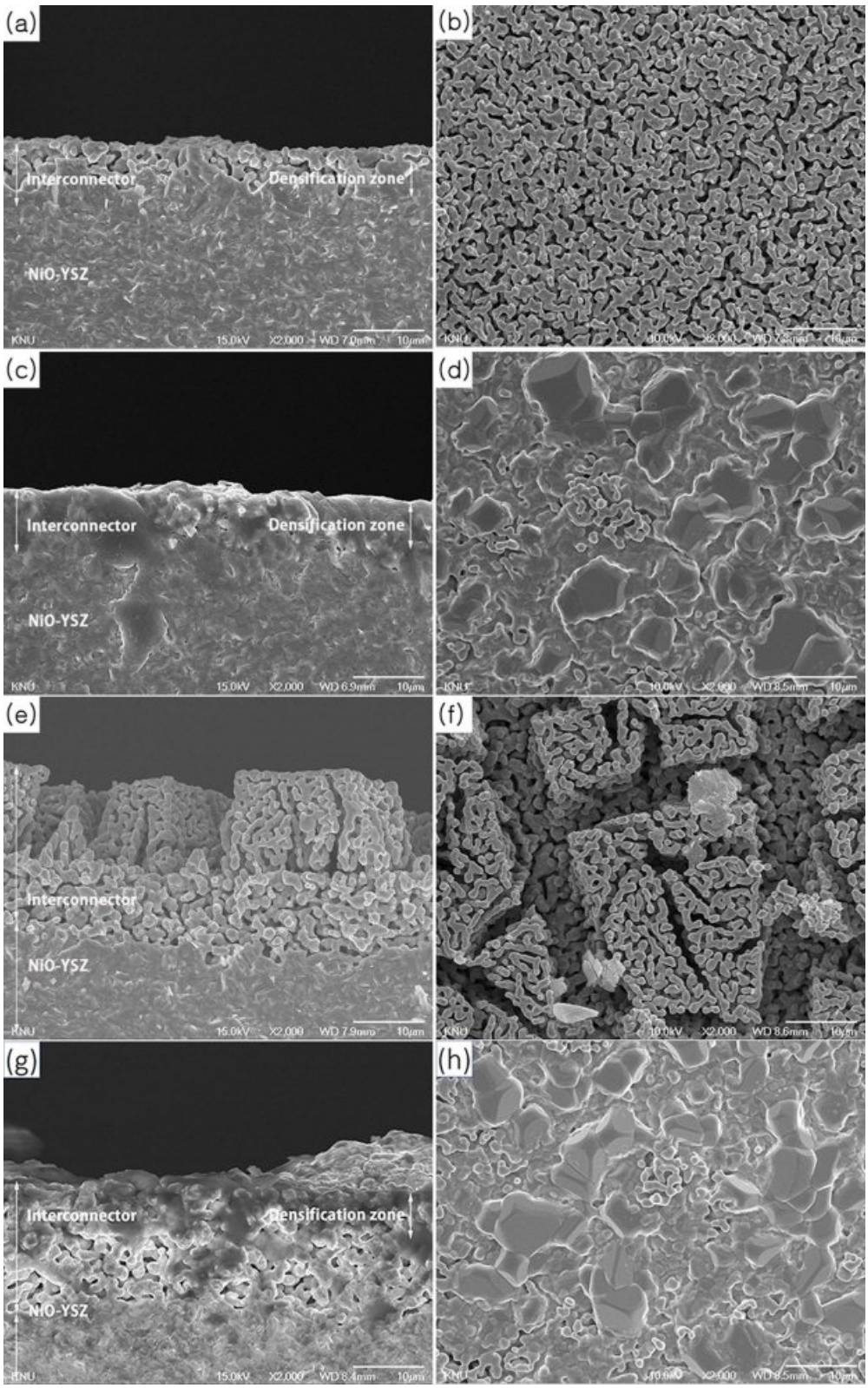


**Fig. 3.** Microstructures at the cross-section (left) and top surface (right). The layers were fired at 1,400 °C for 2 h at a heating rate of (a-f) 1 °C/min and (g-h) 5 °C/min.

## Acknowledgments

This work was supported by the Korea Institute of Energy Technology Evaluation and Planning (KETEP) grant funded by the Korea government (MOTIE) (2019-3010-0324-60, The development of high-efficiency

modular SOFC system with extensible power generation).

## References


1. W.Z. Zhu and S.C. Deevi, Mater. Sci. Eng. A 348 (2003) 227-243.
2. J. Molenda, K. Swierczek, and W. Zajac, J. Power Sources 173 (2007) 657-670.
3. B.K. Park, R.H. Song, S.B. Lee, T.H. Lim, S.J. Park, C.O. Park, and J.W. Lee, J. Kor. Ceram. Soc. 51 (2014) 231-242.
4. N.Q. Minh and T. Takahash, in "Science and technology of ceramic fuel cell, 1st Edition" (Elsevier Science, 1995).
5. S.C. Singhal and K. Kendall, in "High temperature and solid oxide fuel cells: Fundamentals, Design and Applications, 1st Edition" (Elsevier Science, 2004)
6. M. Mori and N.M. Sammes, Solid State Ionics 146 (2002) 301-312.
7. K. Deshpande, A. Mukasyan, and A. Varma, J. Am. Ceram. Soc. 86 (2003) 1149-1154.
8. J. Ovenstone, K.C. Chan, and C.B. Ponton, J. Mater. Sci. 37 (2002) 3315-3322.
9. H.C. Lee, B.K. Kang, J.H. Lee, Y.W. Heo, J.Y. Kim, and J.J. Kim, Ceram. Int. 39 (2013) 8737-8741.
10. E.A. Lee, S. Lee, H.J. Hwang, and J.W. Moon, J. Power Sources 157 (2006) 709-713.
11. E.A. Lee, J.S. Yoon, H.J Hwang, J.W. Moon, and N.U. Cho, J. Ceram. Process. Res 9 (2008) 538-543
12. P. Plonczak, M. Joost, J. Hjelm, and M. Søgaard, J. Power Sources 196 (2011) 1156-1162.
13. R. Koc and H.U. Anderson, J. Eur. Ceram. Soc. 9 (1992) 285-292.
14. G.M. Christie, P.H. Middleton, and B.C.H. Steele, J. Eur. Ceram. Soc. 14 (1994) 163-175.
15. H.C. Lee, B.K. Kang, J.H. Lee, Y.W. Heo, J.Y. Kim, and J.J. Kim, J. Kor. Ceram. Soc. 49 (2012) 197-203.